Preparation of oxidized nanocellulose by using potassium dichromate

Kuzieva Makhliyo
Academy of Sciences Republic of Uzbekistan
Atakhanov Abdumutolib
Academy of Sciences Republic of Uzbekistan
Shakhobutdinov Sirojiddin
Academy of Sciences Republic of Uzbekistan
Ashurov Nurbek
Academy of Sciences Republic of Uzbekistan
Yunusov Khaydar (silver4727@yahoo.com)
Academy of Sciences Republic of Uzbekistan
Guohua Jiang
Zhejiang Sci-Tech University

Research Article

Keywords: Carboxyl group, nanocellulose, oxidation, oxidized nanocellulose

Posted Date: September 28th, 2022

DOI: https://doi.org/10.21203/rs.3.rs-2033622/v1

Additional Declarations: No competing interests reported.

Version of Record: A version of this preprint was published at Cellulose on May 9th, 2023. See the published version at https://doi.org/10.1007/s10570-023-05222-8.

Abstract

Nanocellulose (NC) derivatives are being used in a wide variety of high-quality functional applications. One of them is oxidized nanocellulose (ONC), which has been used in biomedical and pharmaceutical applications due to its biodegradable, biocompatible, hemostatic, and antibacterial properties. In this work, ONC was synthesized using potassium dichromate as an oxidizing agent. The structure of ONC was investigated by means of ultraviolet spectrophotometry (UV), fourier transforms infrared spectroscopy (FTIR), X-ray diffraction (XRD), atomic force microscopy (AFM), and thermogravimetric analysis (TGA). The results showed that the primary hydroxyl groups of NC were selectively oxidized to carboxyl groups and their content of 1.36 mmol/g was achieved. The appearance of a new peak (1721 cm^{-1}) in the FTIR- spectra related to the C = O group was observed. The change of ONC degree of crystallinity (DC) from 88.0–82.5% was revealed and the sizes of the unit cells of both NC and ONC were calculated. The thermal stability of ONC decreased compared to NC. The oxidation process of NC leads to a change in the shape and size of particles from acicular to spherical with a narrow particle size distribution. It was shown that ONC has the ability to accumulate charge on its surface.

Introduction

NC is a new modified form of cellulose; it's characterized by a high DC, surface area, degree of dispersion, degradability by microorganisms, etc. Due to their properties such as biocompatibility, biodegradability, and low toxicity, materials based on NC have been widely used in recent years in various fields, including in biomedicine (Lin, and Dufresne 2014, Reshmy et al. 2021, Trache et al. 2020, Sezali et al. 2021, Thomas et al. 2020). NC is obtained from various cellulose-containing raw materials (wood, straw, cotton cellulose, etc.) by hydrolysis with aqueous solutions of inorganic acids, ultrasonic dispersion, microwave irradiation, etc. (Zaini et al. 2013, Atakhanov et al. 2020, Moran et al. 2008, Yang et al. **2012**. A. Atakhanov et al. 2019, Yadav et al. 2021). The surface of the CNCs contains numerous hydroxyl (–OH) groups, which provide the main reaction site for modification. By introducing additional functional groups into the structure of nanocellulose, it becomes possible to regulate its properties and expand the scope of its application (Braun and Dorgan 2009, Hasani et al. 2008, Morandi et al. 2009). Etherification, oxidation, silylation (тшунмадим), and grafting of macromolecules are typical ways (Sun et al. 2015, Salam et al. 2015, Chen et al. 2015, Sun et al. 2014, Kedzior et al. 2016).

The oxidation process of nanocellulose is of scientific interest, since, depending on the reaction conditions, the final product may contain both carbonyl (aldehyde, ketone) and carboxyl groups (Gensh and Bazarnova 2013, Yuldoshev et al. 2016, Huang et al. 2016, Luo et al. 2013). ONC is a new derivative of nanocellulose with unique performance properties. Currently, research is being actively carried out on the development of haemostatic drugs, cosmetic products, and medical implants based on ONC (Czaja **2014**, Isogai 2018**)**. ONC can be also used as a filler or reinforcement in polymer nanocomposites in order to give special properties to materials (Mahendra et al. 2020, Barnes et al. 2019, Gabriel et al. 2022). Furthermore, the NC derivatives based materials have become extensively interesting recently in scientific

and industrial fields as a promising sustainable substrate material for its versatile usage also in flexible energy storage devices Wang et al. 2017, Fang et al. 2014, Zu et al. 2016).

Depending on the type of oxidation and its reaction conditions, ONC samples with different properties can be obtained (Levanic et al. 2020, Besbes et al. 2011, Isogai et al. 2018). One of the most popular chemical pretreatments in the manufacture of NC is oxidation mediated by 2,2,6,6-tetramethylpiperidine-1-oxyl radical (TEMPO) (Isogai et al. 2011). Catalytic oxidation using TEMPO has opened a new direction in effective and selective chemistry for the conversion of cellulose hydroxyl groups into aldehydes, ketones, and carboxyl groups under mild conditions (Isogai 2018, Hassan et al. 2021). To obtain ONCs with a high content of the carboxyl group, the TEMPO-NaBr-NaClO system has been widely used with ultrasonic dispersion at various pH values (Robert et al. 2011, Hondo et al. 2019). In recent years, several other methods of oxidizing cellulose nanoparticles have appeared. So, given the high cost of TEMPO for NC oxidation, a potential alternative of ammonium persulfate (APS) has appeared which makes it possible to synthesize ONC with higher values of DC (Filipova et al 2018, Oun et al. **2018)**. The ONC produced by using the APS-oxidation method showed also superior mechanical properties, and thermal stability compared with the cellulose nanofibrils (CNF) produced by the TEMPO-mediated oxidation method (Oun et al. **2017**, Zhang et al. 2016). However, when APS is used for NC oxidation, the resulting content of carboxyl groups remains lower compared to those when using other methods and a large amount of APS is needed (Yang, et al 2019). So, it's considered the search for new approaches to the oxidation of NC using more accessible reagents under mild conditions is of scientific and practical interest. The aim of this work was to study the oxidation of NC in the presence of potassium dichromate in an acidic medium and study the property and structure of the ONC.

Method

Materials and chemicals

Potassium dichromate ($K_2Cr_2O_7$) was purchased from Sigma-Aldrich (Sweden). Sinopharm Chemical Reagent Company Ltd (China) supplied sulfuric acid. Daejung (South Korea) supplied sodium hydroxide (NaOH, 98%). NC (DP = 120, DC = 88%) was obtained from cotton cellulose (Atakhanov et al. 2020) and used as raw material for preparing ONC. Deionized water was used in all experiments unless otherwise specified.

Preparation of ONC

ONC was prepared in an aqueous medium by using a calculated amount of $K_2Cr_2O_7$ and H_2SO_4, varying the reaction time from 3 hours (sample ONC-3) to 9 hours (sample ONC-9). In a three-neck flask, 3.0 g of dried CNC powder was dispersed in 50 mL of deionized water and treated with the ultrasonic instrument for 20 min. Next, the pH of the suspension was adjusted to 2–3 with sulphuric acid. 3.63 g potassium dichromate was added into the flask and maintained with constant magnetic agitation at a temperature of 40°C in a glycerine bath for 3–9 h, bubbled with nitrogen gas. The product was centrifugated and was

repeatedly washed with deionized water under centrifugation at 8000 rpm for 15 min until a final pH of 5 was obtained in the system. Then the ONC suspension was dialyzed using dialysis membranes in deionized water for 3 days. Finally, the ONC was separated from the suspension by centrifuging and dried in a freeze-dryer for later use.

Characterization of ONC

Fourier transform infrared spectroscopy (FTIR)

IR spectroscopic studies were carried out with an Inventio-S IR Fourier (Bruker, Germany) with a disturbing total internal reflection attachment in the range from 500 cm^{-1} to 4000 cm^{-1}, with a spectral resolution of 0.085 cm^{-1}, and a scanning speed of 2.5 cm^{-1}/ with.)

Ultraviolet spectrophotometry (UV)

UV spectra were recorded with a Specord 210 UV-spectrophotometer (Analytic Jena, Germany) using quartz cells 1 cm in diameter, a scanning area of 190–1000 nm, 1 nm slit, and a scanning speed of 5 nm/s.

X-ray diffraction (XRD)

X-ray studies were carried out with an XRD Miniflex 600 device (Rigaku, Japan) with monochromatic Cu Kα radiation isolated by a nickel filter with a wavelength of 1.5418 Å at 40 kV and a current strength of 15 mA. The samples were examined in the form of a powder. The survey was carried out in the interval $2\theta = 2^{\circ}–70^{\circ}$.

Atomic force microscopy (AFM)

Structural studies were performed using atomic force microscopy with an Agilent 5500 instrument (Agilent, USA). The silicon cantilevers with a stiffness of 9.5 N/m^2 and a frequency of 262 kHz were used. The maximum x-y-z AFM scan area is 25-25-1 μm. The maximum x-y-z AFM scan area is 4.5-4.5-1 μm.

Thermogravimetric analysis (TGA)

Thermal analysis of the samples was carried out with an STA PT1600 TG-DSC/DTA synchronous thermal analyzer (Linseis, Germany) by heating ~ 20 mg of the sample in an air atmosphere from 25°C to 900°C (heating rate 10°C/min).

Dynamic light scattering (DLS)

The particle size of ONC was estimated by dynamic light scattering using a Photocor compact device (Photocor, Russia). The measurements were carried out at a temperature T = 298 K using a thermally stabilized semiconductor laser with a wavelength of 635.6 nm and a power of 25 mW.

Determination of carboxyl group content

The content of carboxyl groups (mmol/g) in the samples was determined by conductometric titration on a Mettler Toledo conductometer (Switzerland). A dried ONC sample (50 mg) was dispersed in 20 ml of 0.01 M HCl solution and stirred for 15 minutes. Then, the suspension was titrated with a 0.01 M NaOH solution. The number of carboxyl groups in the modified fibers was calculated using an equation (Habibi et al. 2006) and expressed in mmol/g. Each batch was titrated three times.

Impedance spectroscopy

The measurements were carried out on thin films deposited on ITO substrates using Metrohm Autolab (Autolab PGSTAT302N, Netherlands), sample area (5.5 mm^2), on which silver paste was applied to ensure the necessary electrical contact between the test sample and the meter. The impedance spectra were obtained in the frequency range of 1 Hz to 106 Hz with scan rates of 10 mV/s. The results were analyzed using the NOVA 2.0 - Advanced electrochemistry software.

Results And Discussion

Reaction analysis

Dichromate solutions have long-term stability in acid, light, and many organic substances and chlorine ions; therefore, they are conveniently used in various chemical reactions. In the course of NC oxidation dichromate ions (Cr^{6+}) are reduced to Cr^{3+}, which changes the color of the solution from orange to green; in this case, firstly the hydroxyl group is oxidized to an aldehyde group and then to carboxyl groups. NC oxidation proceeds heterogeneously. The course of such a process is significantly influenced by the supramolecular structure of NC and its structure.

The amount of carboxyl group in the ONC samples was determined by conductometric titration (Fig. 1).

The titration curves have a parabolic shape when initial decreases in conductivity are related to the neutralization of HCl with NaOH solution due to the accumulation of ions with low mobility (cations and anions). After complete neutralization of free HCl, the conductivity plateaued out where NaOH consumption was associated with the weak carboxylic group on the ONC (Jiang et al. 2013). After reaching the second point of equivalence, the electrical conductivity of the solution increases due to an increase in the concentration of –OH ions with high mobility. Calculations of the results of conductometric titration showed that with an increase in the duration of the reaction, the amount of carboxyl groups increases from 1.21 (for ONC-3) to 1.36 (for ONC-9) mmol/g.

Characterization

FTIR analysis

The formation of carboxyl groups was also confirmed by IR spectroscopic studies (Fig. 2). Comparative studies of NC and ONC showed that absorption bands at ~ 3400 cm^{-1} are observed, which are related to the stretching vibrations of O–H. In the case of ONC, this absorption band narrows and appears more intensely due to a decrease in the number of hydroxyl groups involved in hydrogen bonds. The stretching vibrations of the CH bonds in methylene and methine groups are manifested in the regions of 2800–2950 cm^{-1}. The presence of adsorbed water was observed around 1635 cm^{-1}, the water molecules cannot be total because of cellulose water interaction. (Moran et al. 2008), the absorption bands in the range of 1420 cm^{-1}, 1335–1375 cm^{-1}, 1202 cm^{-1}, 1075–1060 cm^{-1} correspond to the bending vibrations of -CH–, -CH_2–, –OH, and –CO, and the stretching vibrations of C–O and the pyranose rings. In contrast to the spectrum of the NC samples, a new absorption band appears in the FTIR spectra of ONCs at 1721 cm^{-1}, which is related to the stretching vibration C = O, confirming the presence of carboxyl groups. This suggests that the primary hydroxyl groups (on C6) of the anhydroglucose unit were converted into carboxyl groups successfully (Tang et al. 2017, Lin et al. **2018)**. The intensity of ONC-9 is stronger than ONC–3, indicating a higher amount of carboxyl groups and a higher degree of oxidation. At the same time, in the region of 1425 cm^{-1} related to bending vibrations of –CH_2– groups, the signal intensity decreases, and the intensity of the absorption band at 1315 cm^{-1} related to fan-shaped vibrations of –CH_2– groups, which are associated with out-of-plane vibrations, increases. This is because there is a decrease in the degree of crystallinity of the ONC product, which was also confirmed by X-ray diffraction studies (below in the text). At the same time, the pyranose ring of the elementary cellulose unit is preserved, which confirms the oxidation of the C6 hydroxyl group.

The results of UV spectroscopic studies show (Fig. 3) that there are three absorbance maximums at roughly 196, 240, and 290 nm peaks associated with chromophore group C = O of the aldehyde group (at 240, 290 nm) and the carboxyl group (at 190–210 nm). The spectra It is observed an increase in the number of conjugated bonds leads to a bathochromic shift, which is well described by the Woodward rule (Ager et al. **1996**,)

XRD analysis

The crystalline structure is one of the important determining factors for the strength and thermal stability of cellulose. The crystal structures of ONC samples were evaluated by XRD analysis (Segal **1959**). The results of the X-ray study showed that in all samples there are four crystal reflections in the region 2θ = 14°, 16°, 22° and 34°, corresponding to the planes 101, 10 − 1, 002, and 040 (Fig. 4.). DC of ONC was decreased from 88–79% with increasing duration of the oxidation process, which means that the crystal structure of NC is partially destroyed. This also confirms the values of interplanar distances (d), which increase in ONC samples. It is interesting to note that during the TEMPO- oxidation of the initial cellulose to obtain ONC, an increase in the degree of crystallinity is observed, which is explained by the removal of the amorphous parts of cellulose during the oxidation process using strong oxidants (Qin et al. 2011).

The results of X-ray diffraction analysis showed that the oxidation process of NC affects the crystallite size of NC anisotropically, i.e. the crystallite sizes increase in the two directions (a, c) (Table 1)

Table 1
Structural parameters of NC and ONC samples

Options	Samples								
	NC			ONC – 3			ONC–9		
	Crystal Reflexes								
	101	10 – 1	002	101	10 – 1	002	101	10 – 1	002
Position of maximum 2θ, (deg.)	14.89	16.37	22.75	14.75	16.46	22.66	14.74	16.45	22.67
Interplanar distance d, (Å)	5.94	5.37	3.90	5.99	5.38	3.92	6.00	5.38	3.91
Crystallite size l, (Å)	49.6	46.0	73.3	48.3	44.0	65.4	47.2	42.1	61.7
DC, %	88.0			86.0			82.5		
Unit cell size a ÷ b ÷ c (Å)	8.15 ÷ 10.4 ÷ 7.83			8.21 ÷ 10.35 ÷ 7.87			8.64 ÷ 10.15 ÷ 7.92		
Effective crystallite size, a ÷ b ÷ c, (Å)	44.0 ÷ 146.6 ÷ 18.7			39.4 ÷ 130.8 ÷ 24.1			35.6 ÷ 123.4 ÷ 29.1		

We assume the oxidation process begins from the surface of the crystallites and then gradually moves into the deeper layers. Theoretical calculations were carried out and a model was created (Fig. 5) about the available hydroxyl groups for oxidation at carbon C6, which was also shown in the work (Habibi et al. 2006).

According to the sizes of the unit cell and crystallites calculated from the X-ray diffraction analysis data (Table 1), 4819 elementary units of cellulose are located in one NC crystallite. Conditionally assuming that the crystallites have the shape of a quadrangular prism and only considering the hydroxyl groups of the chain at carbon C6, which is more accessible for external modification, we calculated the number of available hydroxyl groups of carbon C6 is 241. That is, if 241 hydroxyl groups are oxidized, the state

oxidation (CO) will be 100%. This is approximately 5% of the total number of hydroxyl groups of the elementary units in the crystallite with the above indicated size. Theoretical calculations showed that 60% of the available hydroxyl groups on the C6 carbon were oxidized to carboxyl groups.

The thermal stability of the samples was shown in TGA curves (Fig. 6). All thermograms display the characteristic behavior of endothermic polymeric degradation. TGA analysis showed that the decomposition temperatures of the ONC samples are decreased compared to that of the NC sample, while the higher the content of the carboxyl groups is, the lower the decomposition temperature. The weight loss for all samples proceeds in three stages. The presence of adsorbed water in the all of samples is indicated by the initial weight of approximately 5–9% (Gabriel et al. 2022).

A further increase in temperature leads to the second stage of the TG curve, accompanied by large values of weight loss, which corresponds to the process of dehydration. However, as shown in Fig. 6, in the first stage, the ONC samples lose more weight than the NC sample.

In this case, the greater the content of the carboxyl groups in the ONC samples, the greater the weight loss. This is probably due to the decomposition process of cellulose, catalysed by carboxyl groups; therefore, it proceeds at 200℃, while in the case of the NC sample, the temperature of the decomposition process is approximately 250 ℃. These data are consistent with the results obtained in other studies (Zhang et al. 2016, Sharma et al. **2014**), where this phenomenon is also explained by a decrease in the degree of crystallinity and the content of the carboxyl groups.

Determining the sizes of nanoparticles is difficult by the unique constraints of the different analytical methods chosen. Several methods such as AFM (Beck-Candanedo et al. **2005)**, transmission electron microscopy (TEM) (Becrean et al. **2000)**, DLS together with dynamic depolarized light scattering (Lima et al. **2002)**, field emission scanning electron microscopy (FESEM) (Hassan et al), are used for determining NC dimensions and morphology. In this work, the sizes and distribution of particles were estimated by the DLS method (Boluk et al 2014), which showed that the sizes of particles ranged from nano- to micrometers, and a polymodal distribution of particles was also observed (Fig. 7, Table 2). NC and ONC are surface-active and easily agglomerated and form micron-sized clusters. The size of the ONC particles decreases with an increased duration of the oxidation process, which is in good agreement with the results of AFM studies (Fig. 8). It was also revealed the oxidation process leads to a narrowing of the distribution of particles, which can be described by the Lorenz distribution.

Table 2
Particle size distributions

Samples	Radius R, nm	Content, %	Dynamic light scattering D_t (m^2/s)
NC	182	98.8	1.342×10^{-12}
ONC–3	127	89.3	1.924×10^{-12}
ONC–9	113	84.5	2.162×10^{-12}

The AFM study showed that NC particles have an acicular shape with a width of 20–80 nm and a length of 180–600 nm (Fig. 8). The oxidation process leads to a decrease in the size of particles with a width of 50–120 nm and a length of 150–400 nm and partial destruction of the acicular shape of NC with a transition to a spherical shape. An increase in the time of the oxidation process leads to the formation of agglomerates of spherical particles with a size of 20–60 nm.

The oxidation process leads to a decrease in the content of larger particles and an increase in the content of fine particles, while the particle size distribution becomes monodisperse.

The study of macromolecular substances by electrochemical impedance spectroscopy is possible due to the correlation between the electrophysical properties observed in the experiment and the molecular structure of the substance. By means of impedance spectroscopic measurements, the dipole moment, polarizability, rotational velocity of a particular group, or of a macromolecule as a whole, i.e., quantities that determine the structure, conformational features, and molecular mobility of a macrochain both in an isolated state and in a condensed state, can be determined.

Studied the electrophysical properties of NC and ONC–9 by impedance spectroscopy, as seen from the experimental data. The Nyquist diagrams for NC and ONC–9 are shown in Fig. 9. In the region of high-frequency values, a capacitive semicircle is partially observed. The semicircle is the result of a combination of resistances, which is polarization resistances, i.e., the sum of the charge transient resistance at the NC/electrode interface and the ONC/electrode in parallel to the total capacitance. A different behaviour was observed at low frequencies, which indicates the good abilities of ONC–9 to accumulate charge on their surfaces. (Natalia et al. 2013, Hernández-Flores et al. 2020),

It can be seen from the phase diagram (Fig. 10) in case of both samples the intensity of the low-frequency region is greater than the high-frequency regin, since the number of segments is less than the number of the elementary link. Increasing the length of the functional group of ONC-9 leads to an increase in intensity and frequency. The response of a polymer to an electric field is the stronger, the

better the dipoles are oriented in it and the larger the dipole moment. (Chan et al. **2018).** Since the dipole moment increases during the transition from NC to ONC.

Conclusion

In summary, the possibility of NC oxidation in a more accessible way under mild conditions using potassium dichromate in an acidic medium was shown. The oxidation of NC proceeds at C6 carbon without the destruction of the pyranose ring of cellulose and the number of carboxyl groups of the ONC is 1.21–1.36 mmol/g. It is revealed that an increasing of the oxidation process duration leads to decreases in the degree of crystallinity and thermal stability. Based on the results of the X-ray structural analysis, the sizes of both the crystallites and the unit cells of NC and ONC are calculated, where a decrease in size in one direction and an increase in size in the other two directions of measurement are observed. Theoretical calculations were carried out, and a model was created for the hydroxyl groups available for oxidation at carbon C6, which amounted to approximately 5% of the total number of hydroxyl groups of the elementary units in the crystallite. It was calculated that 60% of the available hydroxyl groups at carbon C6 were oxidized to carboxyl groups. By using AFM and DLS was showed that the oxidation process leads to a decrease in the particle size and a change in the shape of the particles from acicular to spherical, while the particle size distribution becomes monodisperse. The ONC samples are able to accumulate charge on their surfaces. The ONC formed by potassium dichromate oxidation has potential application as an environmentally friendly and cost-effective nanomaterial in energy-related fields.

Declarations

Acknowledgments We would like to thank academician Sayora Sharafovna director at the Institute of Polymer Chemistry and Physics Uzbekistan Academy of Sciences for supporting with Fundamental Research Program of the Institute of Chemistry and Physics of Polymers of the Academy of Sciences of the Republic of Uzbekistan for the years 2021-2025, “Fundamental aspects of the creation of nanostructured polymer forms of drugs and medical products - the future of nanoparticles in the body”. This work was supported by the applied project of the Ministry of Innovative Development of Uzbekistan grant number A-FA-2021-388.

Author contributions I declare that all the authors had significant participation in the development of this work. K.M conceived the experiments, original draft, A.A Supervision, writing- review & editing, funding acquisition; S.S performed experiments; A.N conceptualization, supervision, writing- review; Y.KH Visualization, writing- review & editing; G.J review & editing. All authors discussed the results.

Declarations Not applicable

Data Availability Not applicable

Consent for publication Not applicable

Availability of data and materials Author/s hereby declares that the raw/processed data required to reproduce these findings cannot be shared at this time due to legal or ethical reasons.

Not applicable

Competing interests Not applicable

Funding Not applicable

Conflict of interest The authors declare that they have no known competing financial interests or personal relationships that could have appeared to influence the work reported in this paper.

References

1. Atakhanov A, Mamadiyorov B, Kuzieva M, Yugay S, Shahobutdinov S, Ashurov N, Abdurazzakov M (2019) Comparative studies of the physicochemical properties and structure of cotton cellulose and its modified forms. *Chem Plant Raw Mater 3:*5. http://dx.doi.org/10.14258/jcprm.2019034554
2. Atakhanov A, Kholmuminov A, Turdikulov I, Mamadiyorov B, Ashurov N (2020) Polym Sci Ser A *62:*3 213.
3. Ager DJ, Michael East B (1996) Chapter: Reactions with carbonyl compounds CRC Press 512.
4. Braun B, Dorgan JR (2009) Single-step method for the isolation and surface functionalization of cellulosic nanowhiskers. *Biomacromol 10*:334. https://doi.org/10.1021/bm8011117
5. Barnes E, Jefcoat JA, Alberts EM (2019) Effect of cellulose nanofibrils and TEMPO-mediated oxidized cellulose nanofibrils on the physical and mechanical properties of poly (vinylidene fluoride)/cellulose nanofibril composites. *Polymers 11*:1091. https://doi.org/10.3390/polym11071091
6. Besbes I, Alila S, Boufi S (2011) Nanofibrillated cellulose from TEMPO-oxidized eucalyptus fibres: effect of the carboxyl content. *Carbohydr Polym 84*:975. https://doi.org/10.1016/j.carbpol.2010.12.052
7. Boluk Y, Danumah C (2014) *J NanopartRes 16*:2174
8. Beck-Candanedo S, Roman M, Gray DG (2005) Effect of reaction conditions on the properties and behavior of wood cellulose nanocrystal suspensions. *Biomacromol. 6* 2:1048. https://doi.org/10.1021/bm049300p
9. Chen J, Lin N, Huang J, Dufresne A (2015) Highly alkynyl-functionalization of cellulose nanocrystals and advanced nanocomposites thereof via click chemistry. *Polym.Chem 6*:4385 https://doi.org/10.1039/c5py00367a
10. Czaja W, Kyryliouk D, Paula CA, Buechter DD (2014) Oxidation of γ-irradiated microbial cellulose results in bioresorbable, highly conformable biomaterial. *J.Appl.Polym.Sci 131*:39995. https://doi.org/10.1002/app.39995

11. Chan ChH, Kammer HW (2018) Characterization of polymer electrolytes by dielectric response using electrochemical impedance spectroscopy. *Pure Appl Chem*. *90:*939 https://doi.org/10.1515/pac-2017-0911
12. De Souza Lima M.M., J.T. Wong, M. Paillet, R. Borsali, R. Pecora (2002) Translational and rotational dynamics of rodlike cellulose whiskers *Langm. 19*.1:24 https://doi.org/10.1021/la020475z
13. Filipova I, Fridrihsone V, Cabulis U, Berzins A (2018) Synthesis of Nanofibrillated Cellulose by Combined Ammonium Persulphate Treatment with Ultrasound and Mechanical Processing *Nanomater*. *8*:9 https://doi.org/10.3390/nano8090640
14. Fang Z, Zhu H, Yuan Y, Ha D, Zhu S, Preston C, Chen Q, Li Y, Han X., Lee S, Chen G, Li T, Munday J, Huang J, Hu L (2014) Novel nanostructured paper with ultrahigh transparency and ultrahigh haze for solar cells. *Nano letters 14*:765 https://doi.org/10.1021/nl404101p
15. Gensh KV, Bazarnova N.G (2013) *Chem. Plant Raw Mater*, *4*:13.
16. Gabriel VA, Champagne P, Cunningham MF, Dubé MA (2022) In-situ addition of carboxylated cellulose nanocrystals in seeded semi-batch emulsion polymerization. *Can. J. Chem. Eng. 100,* 4, 767. https://doi.org/10.1002/cjce.24299
17. Hassan S.H, T.S. Velayutham, Y.W. Chen, H.V. Lee (2021) TEMPO-oxidized nanocellulose films derived from coconut residues: Physicochemical, mechanical and electrical propertie. *Int. J. Biol*. Macromol *180*, 392 https://doi.org/10.1016/j.ijbiomac.2021.03.066
18. Hasani M, Cranston ED, Westman G, D.G. Gray (2008) Cationic surface functionalization of cellulose nanocrystals. *Soft Matter*., *4*, 2238. https://doi.org/10.1039/B806789A
19. Huang R., Liu, Z, Sun, B., Fatehi, P (2016) Preparation of dialdehyde cellulose nanocrystal as an adsorbent for creatinine. Can. J. Chem. Eng., 94(8), 1435–1441. https://doi.org/10.1002/cjce.22523
20. Hondo H, Saito T, Isogai A (2019) Preparation of oxidized celluloses in a TEMPO/NaBr system using different chlorine reagents in water. *Cellulose 26*:3021 https://link.springer.com/article/10.1007/s10570-019-02311-5
21. Habibi Y., H. Chanzy, M.R. Vignon (2006) TEMPO-mediated surface oxidation of cellulose whiskers, *13*:679. *Cellulose*. https://doi.org/10.1007/s10570-006-9075-y
22. Hassan S.H., T.S. Velayutham, Y.W. Chen, H.V. Lee (2021). TEMPO-oxidized nanocellulose films derived from coconut residues: Physicochemical, mechanical and electrical properties. *Int.J Biolog Macromol 180:*392 https://doi.org/10.1016/j.ijbiomac.2021.03.066
23. Hernández-Flores J.A. Morales-Cepeda A.B, C.F. Castro-Guerrero, F. Delgado-Arroyo, M.R. Díaz-Guillén, J. Cruz-Soto, L. Magallón-Cacho, U. León-Silva (2020) Morphological and electrical properties of nanocellulose compounds and its application on capacitor assembly. *Int .J Pol Sci 2020:*1891064 https://doi.org/10.1155/2020/1891064
24. Isogai A (2018) Development of completely dispersed cellulose nanofibers *Proc. Japan. Acad. Ser. B. Phys. Biol. Sci*., *94*, 4:161. https://doi.org/10.2183/pjab.94.012
25. Isogai A, Hänninen T, Fujisawa S, Saito T (2018) Review: Catalytic oxidation of cellulose with nitroxyl radicals under aqueous conditions *Prog. Polym. Sci*. *86:*122

https://doi.org/10.1016/j.progpolymsci.2018.07.007

26. Isogai A., S. Saito, H. Fukuzumi (2011) TEMPO-oxidized cellulose nanofibers. *Nanoscale.3*:1 https://doi.org/10.1039/C0NR00583E
27. Jiang F., S. Han, Y. Hsieh (2013) Controlled defibrillation of rice straw cellulose and self-assembly of cellulose nanofibrils into highly crystalline fibrous materials† .*RSC Advanc 3:*12366. https://doi.org/10.1039/c3ra41646a
28. Kargarzadeh H, Ahmad I, Abdullah I (2012) Effects of hydrolysis conditions on the morphology, crystallinity, and thermal stability of cellulose nanocrystals extracted from kenaf bast fibers. *Cellulose. 19:* 855
29. Kedzior S.A., L. Graham, C. Moorlag, B.M. Dooley, E.D. Cranston (2016) Poly (methyl methacrylate)-grafted cellulose nanocrystals: One-step synthesis, nanocomposite preparation, and characterization. *Can. J. Chem. Eng. 94*:811. https://doi.org/10.1002/cjce.22456
30. Luo H., G. Xiong, D. Hu, K. Ren, F. Yao, Y. Zhu (2013). Characterization of TEMPO-oxidized bacterial cellulose scaffolds for tissue engineering applications *Mater. Chem. Phys 143*. http://dx.doi.org/10.1016/j.matchemphys.2013.09.012;
31. Levanic J, Petrovič Šenk V, Nadrah P, Poljanšek I, Oven P, Haapala A (2020) Analyzing TEMPO-oxidized cellulose fiber morphology: new insights into optimization of the oxidation process and nanocellulose dispersion quality. *ACS Sustain.Chem. Eng.*, *8*, 48, 17752 https://doi.org/10.1021/acssuschemeng.0c05989
32. Lin N, Dufresne A, (2014) Nanocellulose in biomedicine:Current status and future prospect. *Eur. Polym. J.* 59: 302–325. https://doi.org/10.1016/j.eurpolymj.2014.07.025
33. Lin Ch., T. Zeng, Q. Wang, L. Huang, Y. Ni. F. Huang, X. Ma, S. Cao (2018) Effects of the conditions of the TEMPO/NaBr/NaClO system on carboxyl groups, degree of polymerization, and yield of the oxidized cellulose, *BioResour. 13* 3:5965
34. Morandi G, Heath L, Thielemans W (2009) Cellulose nanocrystals grafted with polystyrene chains through surface-initiated atom transfer radical polymerization (SI-ATRP). *Langmuir.25*:8280. https://doi.org/10.1021/la900452a
35. Moran J.I., Alvarez V.A., Cyras V.P., Vazquez A. (2008) Extraction of cellulose and preparation of nanocellulose from sisal fibers. *Cellulose. 15:*149. https://doi.org/10.1007/s10570-007-9145-9
36. Mahendra I.P., B. Wirjosentono, T. Tamrin, H. Ismail, J.A. Mendez, V. Causin (2020) *J Thermoplast.Comp.Mat.* 1.
37. Moran JI, Alvarez VA, Cyras VP, (2008) Extraction of cellulose and preparation of nanocellulose from sisal fibers, *Cellulose. 15:149 https://doi.org/10.1007/s10570-007-9145-9*
38. Natalia M, Sudhakar YN, Selvakumar M (2013) Activated carbon derived from natural sources and electrochemical capacitance of double layer capacitor. *Ind.J.Chem.Tech. 20, 6*:392
39. Oun AA, Rhim JW (2018) Isolation of oxidized nanocellulose from rice straw using the ammonium persulfate method *Cellulose. 25*:2143 https://doi.org/10.1007/s10570-018-1730-6

40. Oun, A.A J-W. Rhim (2017) Characterization of carboxymethyl cellulose-based nanocomposite films reinforced with oxidized nanocellulose isolated using ammonium persulfate method *Carbohyd. Polym. 174*, 484 https://doi.org/10.1016/j.carbpol.2017.06.121
41. Qin ZY, Tong G L, Chin YCF, Zhou JCh (2011) *Bio Res.*, *6*, 2, 1136
42. Robert J. Moon, Martini A, Nairn J, Simonsen J, Youngblood J. (2011) Cellulose nanomaterials review: structure, properties and nanocomposites *Chem. Soc. Rev*. *40*:3941. https://doi.org/10.1039/C0CS00108B
43. Reshmy R, Philip E, Madhavan A, Arun KB Binod P, Pugazhendhi A, Awasthi MK, Gnansoun E, Pandey A, Sindhu R (2021) Promising eco-friendly materials for future biomedicine: Cleaner production and applications of nanocellulose. *Env.Tech. & Innov 24*:101855 https://doi.org/10.1016/j.eti.2021.101855
44. Sezali NAA, Ong HL,.Jullok N, Villagracia AR,.Doong R-A (2021) A Review on nanocellulose and its application in supercapacitors. *Macromol. Mater. Eng. 306*:2100556. https://doi.org/10.1002/mame.202100556
45. Sun B, Q. Hou, Liu Z (2015) Sodium periodate oxidation of cellulose nanocrystal and its application as a paper wet strengh additive. *Cellulose. 22*:1135. https://doi.org/10.1007/s10570-015-0575-5
46. Salam A, Lucia LA, Jamee H (2015) Fluorine-based surface decorated cellulose nanocrystals as potential hydrophobic and oleophobic materials *Cellulose*. *22*:397 https://doi.org/10.1007/s10570-014-0507-9
47. Sun B, Hou Q, Liu Z, Ni Y (2014). Stability and efficiency improvement of ASA in internal sizing of cellulosic paper by using cationically modified cellulose nanocrystals. *Cellulose. 21*:2879 http://dx.doi.org/10.1007/s10570-014-0283-6
48. Segal L., J. Creely, A.Jr. Martin, C. Conrad (1959) An empirical method for estimating the degree of crystallinity of native cellulose using the X-Ray Diffractometer. *Text. Res. J. 29*;786 http://dx.doi.org/10.1177/004051755902901003
49. Sharma PR, Varma A.J (2014) Thermal stability of cellulose and their nanopa rticles: effect of incremental increases in carboxyl and aldehyde groups *Carbohydr. Polym.*114:339. https://doi.org/10.1016/j.carbpol.2014.08.032
50. Tang Z, Li W, Lin X, Xiao H, Miao Q, Huang L, Chen L, Wu H (2017) TEMPO-Oxidized cellulose with high degree of oxidation *Polymers 9*, 9:421. https://doi.org/10.3390/polym9090421
51. Trache D, Tarchoun AF, Derradji M, Hamidon TS, Masruchin N, Brosse N, Hussin MH (2020) Nanocellulose: from fundamentals to advanced application. *Front. Chem*. *8*:392. https://doi.org/10.3389/fchem.2020.00392
52. Thomas P, Duolikun T, Rumjit NP, Moosavi S, Lai CW, Bin Johan MR, Fen L.B (2020) Comprehensive review on nanocellulose: Recent developments, challenges and future prospects. *J* Mech. Behav. Biomed. Mater *110*:103884. https://doi.org/10.1016/j.jmbbm.2020.103884
53. Wang X, Yao Ch, Wang F, Li Zh (2017) Cellulose-based nanomaterials for energy applications. *Small 13*:1702240 doi.org/10.1002/smll.201702240

54. Yang Yu. M. Huang R, Cao L, Yang X, Liu F (2012) Preparation and characterization of bamboo nanocrystalline cellulose. *BioRes. 7.* 2:1802. https://doi.org/10.15376/biores.7.2.1802-1812
55. Yadav C, Saini A, Zhang W, You X, Chauhan I, Mohanty P, Li X (2021) Plant-based nanocellulose: A review of routine and recent preparation methods with current progress in its applications as rheology modifier and 3D bioprinting. *Int.J.Biol.Macromol. 1,* 166:1586 doi: 10.1016/j.ijbiomac.2020.11.038.
56. Yuldoshev ShA, Atakhanov AA, Sarimsakov AA (2016) Nano Sci. Nano Tech. Ind. J. *3*:102.
57. Yang H, Zhang Y, Kato R, Rowan Stuart J (2019) Preparation of cellulose nanofibers from Miscanthus x. Giganteus by ammonium persulfate oxidation. *Carbohydr Polym 212*:30 https://doi.org/10.1016/j.carbpol.2019.02.008
58. Zhang K, Sun P, Liu H, Shang S, Song J, Wang D (2016) *Carbohyd. Polym. 138:*237 https://doi.org/10.1016/j .carbpol.2015.11.08
59. Zaini LH, Jonoobi M, Md Tahir P, S. Karimi *J* (2013) Isolation and characterization of cellulose whiskers from kenaf bast fibers. *Biomater. Nanotech. 4*:37 https://doi.org/10.4236/jbnb.2013.41006
60. Zu G, Shen J, Zou L, Wang F, Wang X, Zhang Y,. Yao X (2016) Nanocellulose-derived highly porous carbon aerogels for supercapacitors. *Carbon. 99:*203 https://doi.org/10.1016/j.carbon.2015.11.079

Scheme 1

Scheme 1 is available in Supplementary Files section.

Figures

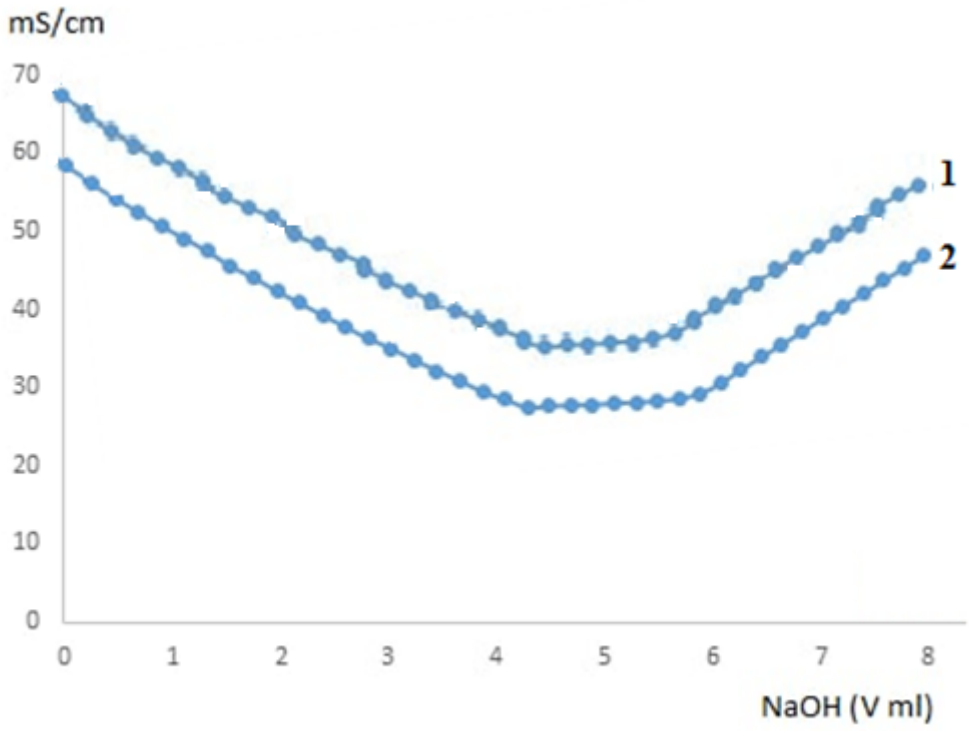

Figure 1

Conductometric titration curves of ONC-3 (1) and ONC-9 (2)

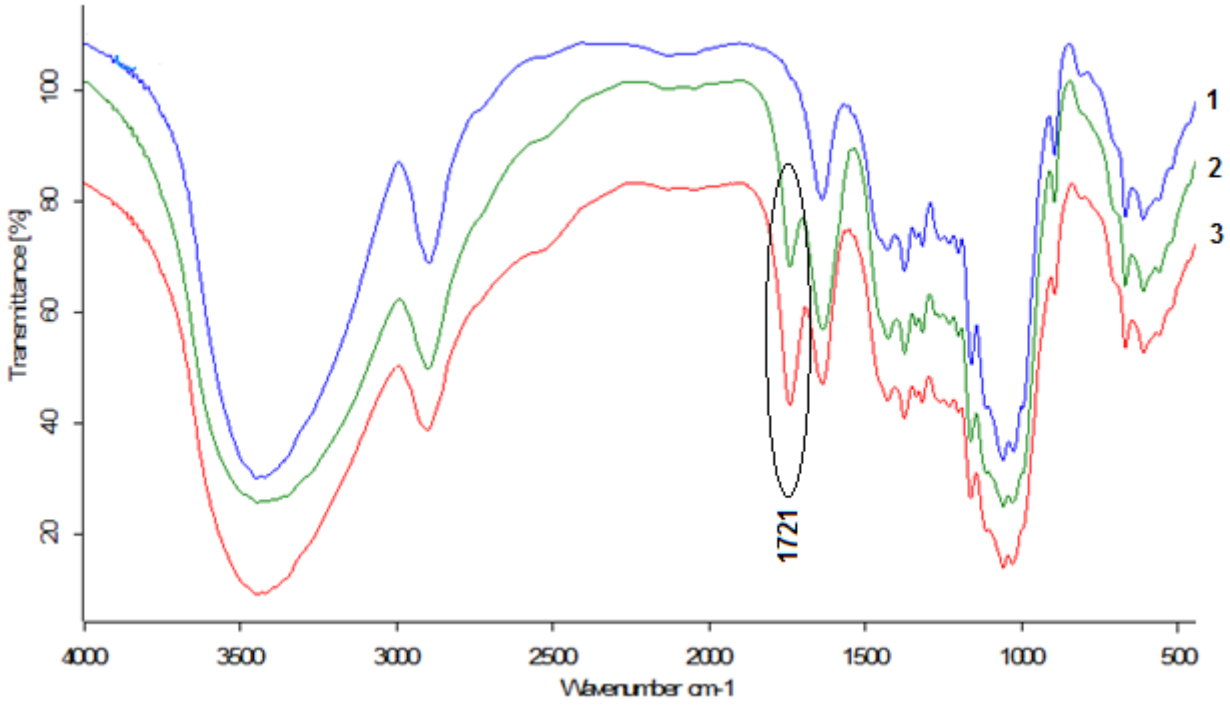

Figure 2

IR spectra of NC–1 (1), ONC–3 (2) and ONC–9 (3).

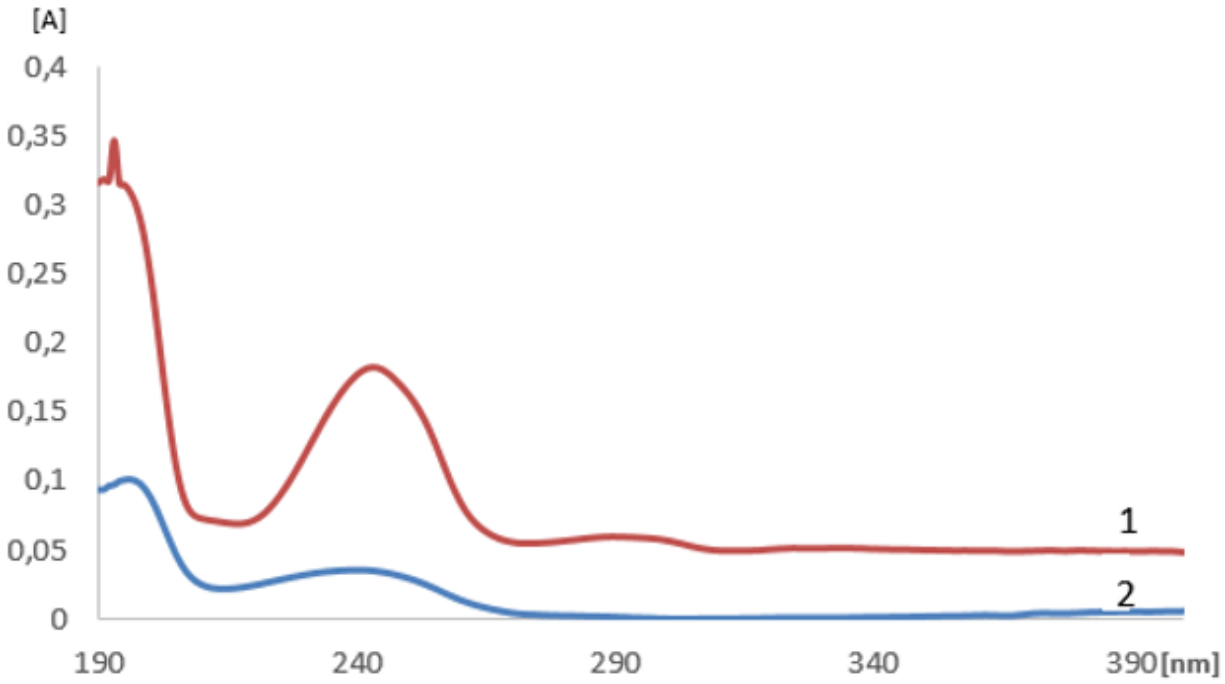

Figure 3

UV spectra of the ONC–9 (1) and ONC 3 (2) samples.

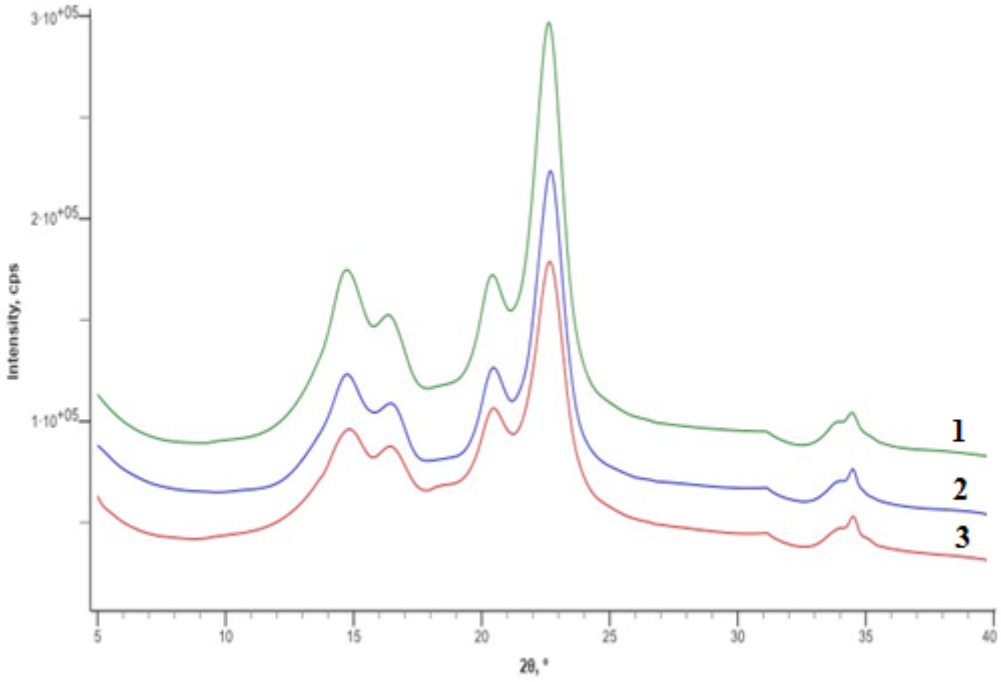

Figure 4

X-ray diffraction patterns of NC (1), ONC-3 (2) and ONC-9 (3).

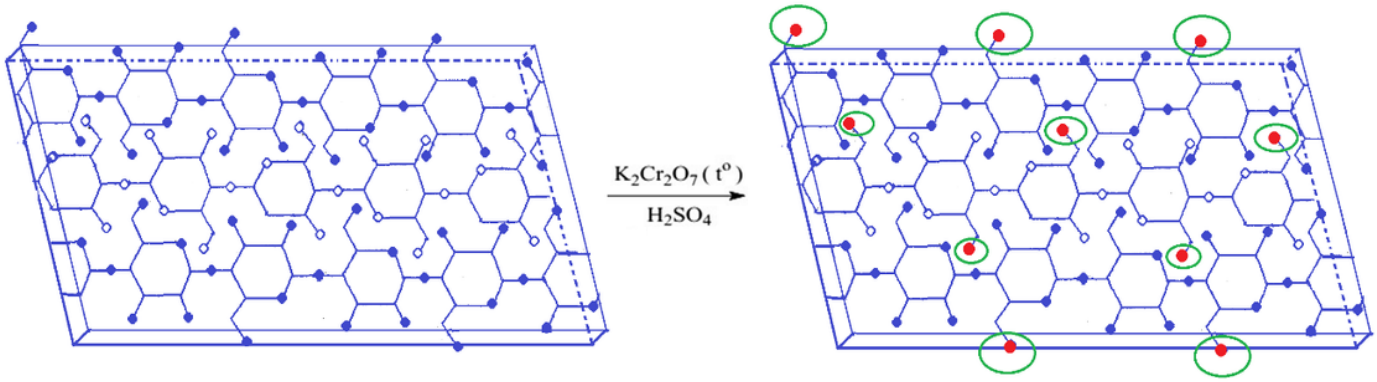

Figure 5

Schematic representation of available cellulose anhydroglucose units on crystallites.

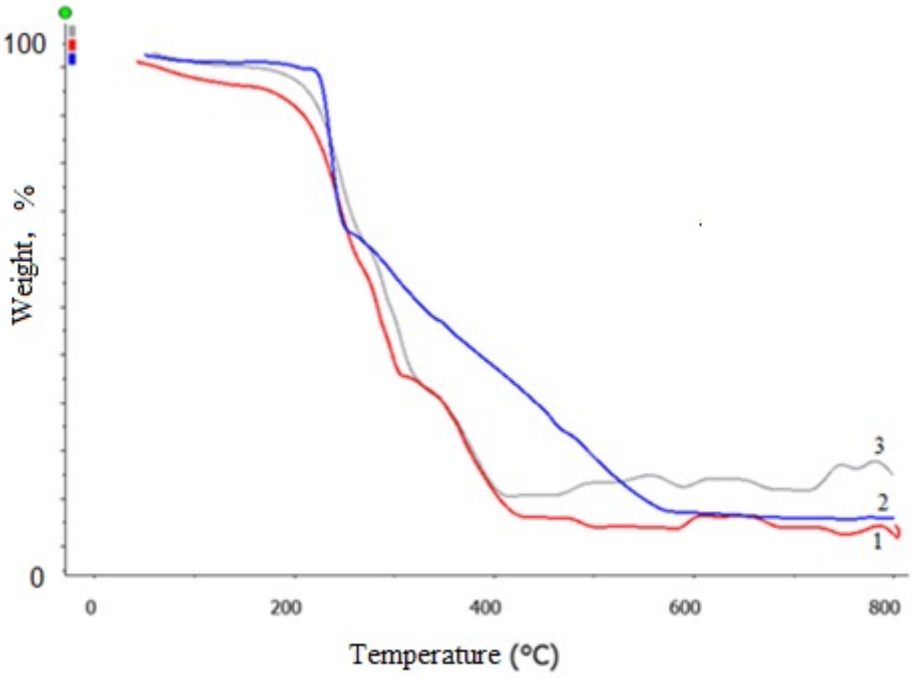

Figure 6

Thermograms of ONC–9 (1), NC (2), ONC–3 (3)

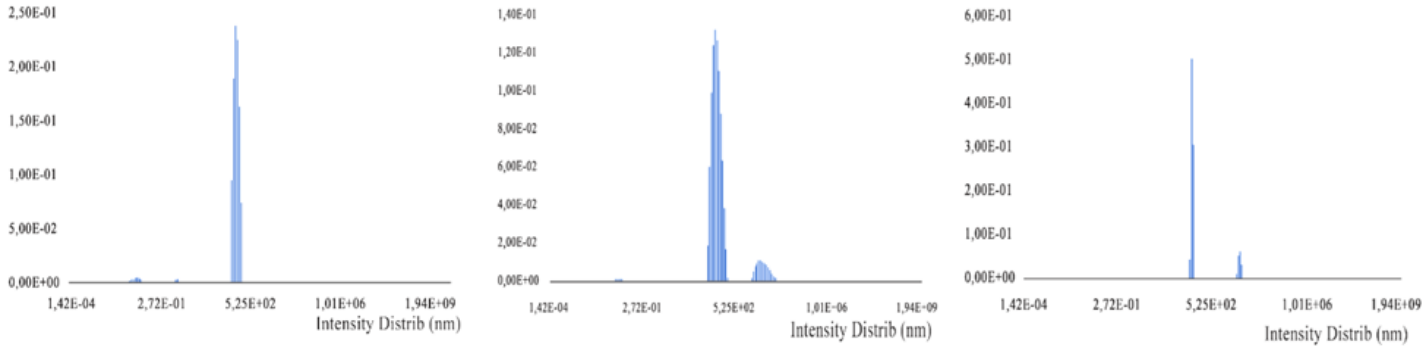

Figure 7

Results of the DLS analysis of NC (a), ONC–3 (b), and ONC–9 (c).

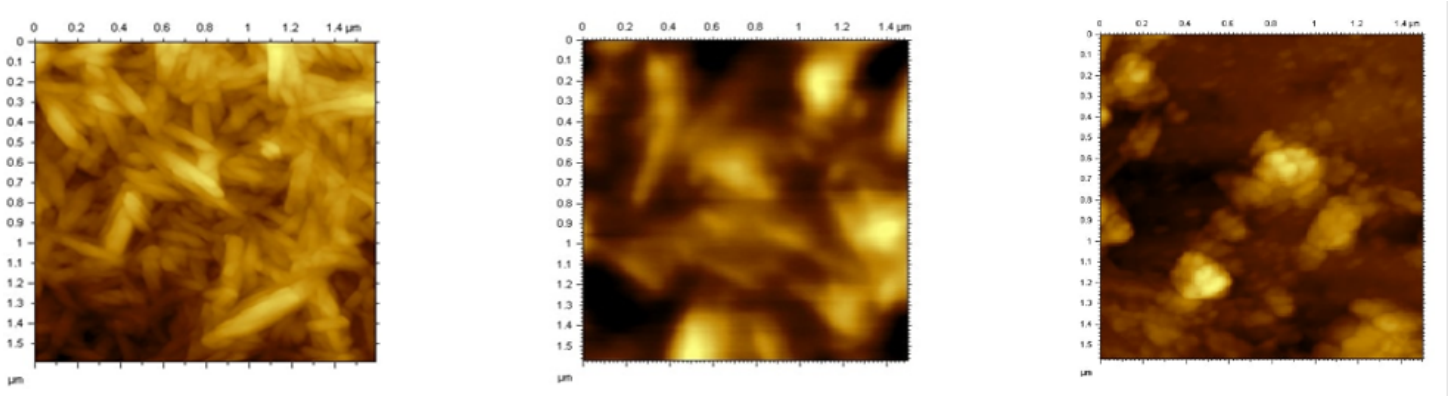

Figure 8

AFM images of NC, ONC–3, ONC–9.

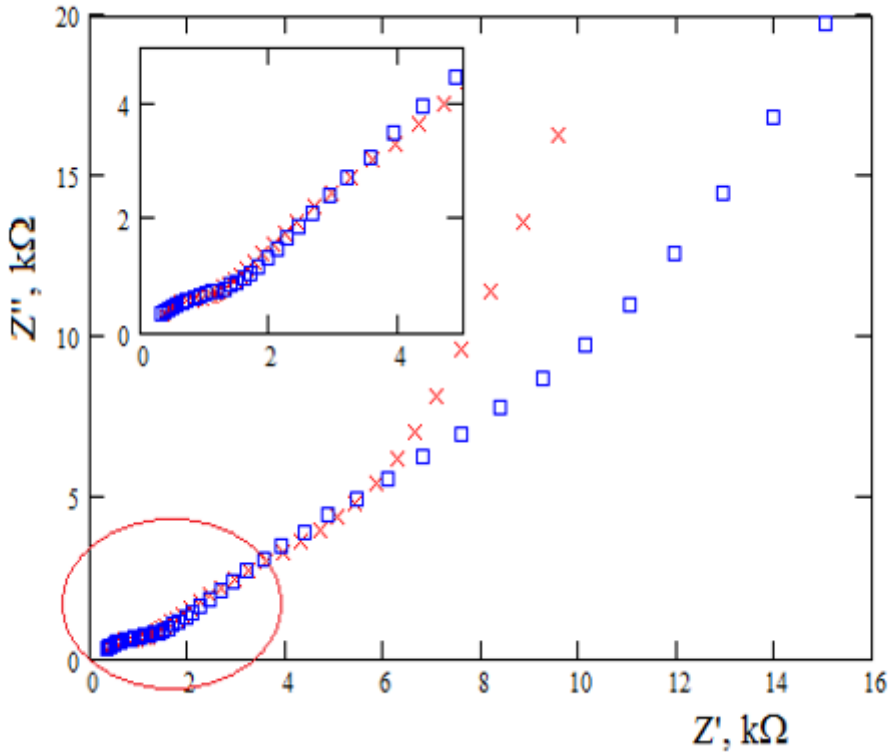

Figure 9

Nyquist diagrams of NC and ONC–9.

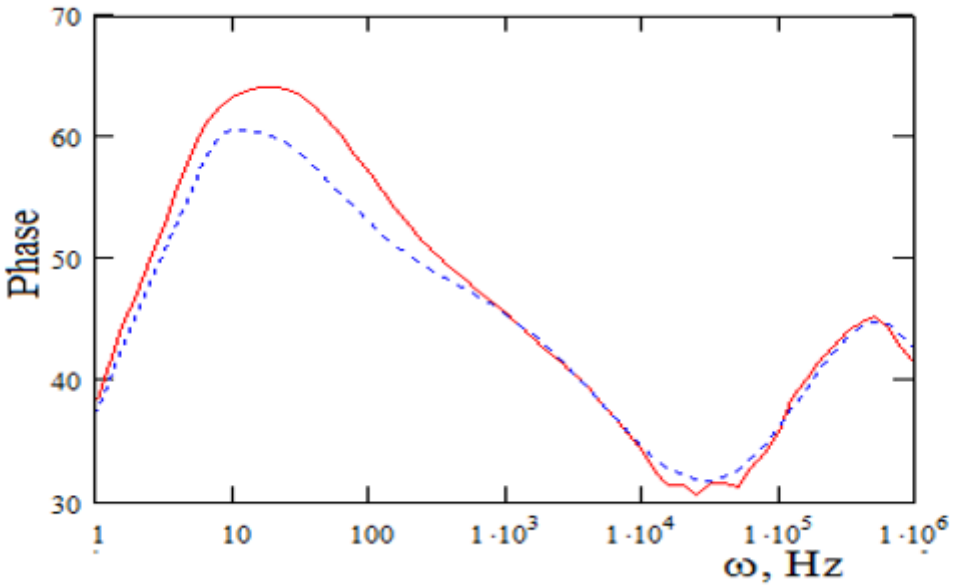

Figure 10

Diagram Bode NC and ONC–9.

Supplementary Files

This is a list of supplementary files associated with this preprint. Click to download.

- Scheme1.png